Modeling Spatial Dependence of Rods and Cones in the Retina

Noah Chicoine[1], Caroline Hammond[2], Anton Iatcenko[3], Luis Schneegans[4], Frederick Senya[5], Lan Trinh[6], Lawan Wijayasooriya[7], and Yuehui Xu[8]

[1]Northeastern University, Boston MA, USA
[2]Dartmouth College, Hanover NH, USA
[3]Simon Fraser University, Burnaby BC, Canada
[4]Stanford University, Stanford CA, USA
[5]University of Vermont, Burlington VT,USA
[6]Tulane University, New Orleans LA, USA
[7]Georgia State University, Atlanta GA, USA
[8]IUPUI, Indianapolis IN, USA

June 23, 2024

Abstract: We develop a Partial Differential Equation (PDE) model for photoreceptors in the retina. We focus on the outer segment (OS) dynamics of rods, cones and their interactions with a nutrient source associated with the retinal pigment epithelium (RPE) cells. Prior models have captured the spatial dependence of the rod and cone photoreceptor density and nutrient diffusion. In addition to that, we have also considered the spatial dependence of photoreceptor outer segment length on retinal thickness in our new model (Model 1). The new model was fitted to biological data using different forms of the functions l_{rH} and l_{cH}, the photoreceptors' mathematical dependency on retinal thickness. Additionally, we found analytical solutions for Model 1. We non-dimensionalized the model, while noting the parameters/variables that were spatially dependent. Dimensionalizing our model with respect to the spatially dependent terms, we were able to find a nontrivial steady-state solution, in addition to our trivial solution. Verification with the optimized parameters and data fitting could show us how our steady-state solution works. Finally, an entirely new model (Model 2) was developed to model photoreceptor OS length as a density function that is dependent on space in time. This model was developed and fitted to biological data of an experiment of retinal detachment and re-attachment. Our work primarily focuses on healthy human eye. However, our models may be useful in providing insights for various retinal pathologies, eye-related injuries, and treatments of these conditions.

1 Introduction

The retina is a thin but complex layer of cells in the back of the eye that is critical to providing humans and other animals with vision. In the retina, two types of photoreceptors, rods and cones, process the light that passes into the eye and send neurological signals to the brain via the optic nerve. Rods are responsible for perceiving objects in low light environments and in the peripheral vision. Inversely, cones are responsible for day vision, color vision, and visual acuity. Billions of rods and cones are dispersed through the retina, which spans most of the inner surface area of the eye (see Figure 1a). photoreceptors are most concentrated at the *fovea*, a divot in the retina at the back of the eye.

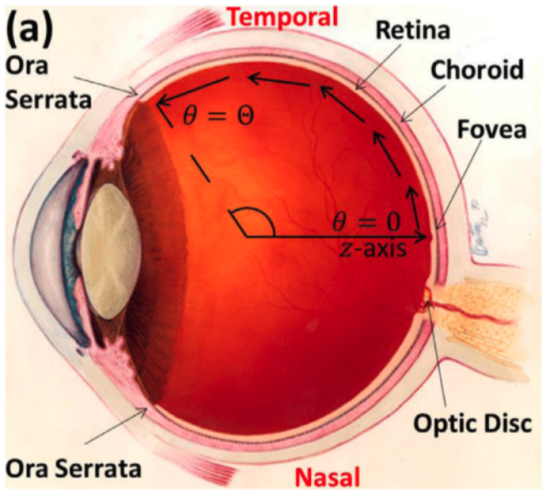

(a) Anatomy of the eye. Figure adopted from Roberts et al. 2017.

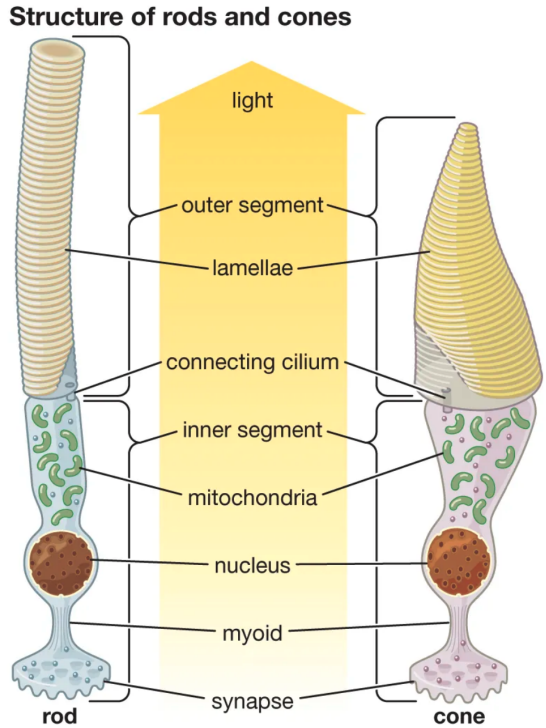

(b) Structure of rods and cones in the retina. The outer segment portion continually goes through generation (at the bottom) and generation (at the top. Figure adopted from *photoreception* n.d.

Figure 1: Anatomy of the human eye.

There are multiple kinds of diseases associated with the retina, including retinitis pigmentosa and macular degeneration, which effect the growth and density of photoreceptors in the eye. These diseases, along with instances of retinal injuries, have inspired scientists to develop mathematical models of different photoreceptor and retina qualities. For example, Roberts et al. 2017 modeled both rod and cone density along the retina. Additionally, they created a kinetic partial differential equations (PDE) model of oxygen diffusion in the retina to test the hypothesis of oxygen toxicity leading to retinitis pigmentosa. In later studies, the authors developed a second model to test a second hypothesis related to a protein called tropic factor (Roberts 2022a; Roberts 2022b). Camacho and Wirkus 2013 developed a kinetic model of the growth and shedding of *outer segments* of rods and cones. The outer segments of rods and cones (see Figure 1b) are critical to the transmission of signals to the retinal pigment epithelium and eventually, the optic nerve. These parts of photoreceptors undergo continuous shedding and renewal as a result of oxidative stress endured during the daytime. The authors used this model to study possible dynamics that can lead to retinitis pigmentosa.

In a more recent paper, D. M. Anderson, Brager, and Kearsley 2024 created a PDE model that expands on those from Camacho and Wirkus 2013 and Roberts et al. 2017 to account for the spatial

dependence of rods and cones throughout the retina. In the retina, cones are typically concentrated at the fovia, while rods tend to lie farther away. While the author's model accounts for this nature, there are additional spacial dependencies that have been noted in literature. Wilk et al. 2017 notes how in areas of high concentrations of photoreceptors, the photoreceptors tend to be longer in length due to the compression caused by other nearby receptors. Additionally, the thickness of the retina changes as a function of distance away from the fovia Kolb, Fernandez, and Nelson 1995, which also potentially impacts the height and growth of retinas. Currently, models do not incorporate retinal thickness, nor do they consider the heterogeneity of photoreceptor outer segment length within small regions of the eye. This potential expansion was the inspiration for the work shown in this report.

In the following sections, we present two new models that could be used in future investigations of retinal pathology or could inspire future biological studies that focus on important mechanisms for photoreceptor regulation in the eye. The first model is an adaptation from D. M. Anderson, Brager, and Kearsley 2024 that incorporates retinal thickness, and represents photoreceptor outer segment length as a function of retinal thickness at each point on the retina. The second model is a new model of spatial dependence of photoreceptors in the eye that models outer segment length of photoreceptors as a heterogeneous distribution of lengths that vary with time and distance from the fovia. With these models, we present analysis of steady state conditions and results from fitting the models to data shown in previous studies. Finally, we present directions for future work.

2 Model 1 Development

2.1 Proposed Model

From Wilk et al. 2017, one could see the thickness of retina around fovia is thinner than the part that is farther from fovia. However, the cones outer segment length becomes shorter as the radia distance increase. Here we are proposing a model that take the thickness of retina into consideration. Instead of considering l_c and l_r as two constant length scale, we are going to introduce l_{rH} and l_{cH}, which depends on the retina thickness $H(\theta)$.

Let $r(\theta, t)$ be the rod outer segment length, $c(\theta, t)$ be the cone outer segment length, $T(\theta, t)$ be the Diffusible nutrient concentration, $R(\theta)$ be the Rod density (per unit area) and $C(\theta)$ be the Cone density (per unit area). Refer to (D. M. Anderson, Brager, and Kearsley 2024) for a detailed derivation and explanation of model interactions.

Consider the following assumptions:

1. Retina thickness is a function of radia distance (θ)
2. Retina thickness and outer segment length are inversely related

$$\frac{\partial r}{\partial t} = a_r r \left(l_{rH} - r\right) T - \mu_r r \tag{1}$$

$$\frac{\partial c}{\partial t} = a_c c \left(l_{cH} - c\right) T - \mu_c c \tag{2}$$

$$\frac{\partial T}{\partial t} = T(\Gamma - kT) - \beta T(l_{rH} - r) r R(\theta) - \gamma T(l_{cH} - c) c C(\theta) \tag{3}$$

where

$$l_{rH} = \alpha_1 H(\theta)[1 - \alpha_2 H(\theta)] \qquad \text{and} \qquad l_{cH} = \alpha_3 H(\theta)[1 - \alpha_4 H(\theta)]$$

2.2 Fitting $H(\theta)$

Though the steady state solution can be found regardless of the form of $H(\theta)$ (shown below), a functional form of $H(\theta)$ was needed to fully parameterize the model so that it could be fitted and tested against biological data. To find $H(\theta)$, the thickness of the retina in terms of distance from the fovia, data was obtained from figures in Liu, Kocaoglu, and Miller 2016, Wilk et al. 2017, and Kolb, Fernandez, and Nelson 1995. Images of the retinas from Liu, Kocaoglu, and Miller 2016 and Wilk et al. 2017 are shown below in Figure 2. MATLAB's *GrabIt* toolbox was used to extract the thickness of the retinas at several points.

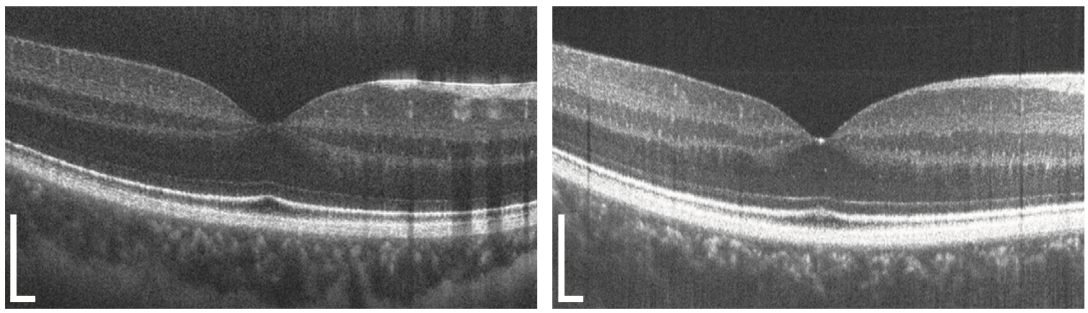

(a) Pictures of two retinas from subjects in Wilk et al. 2017.

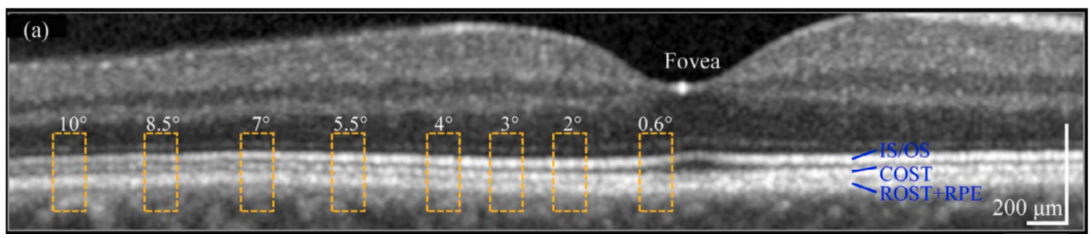

(b) Picture of one retina from a subject in Liu, Kocaoglu, and Miller 2016

Figure 2: Images of retinas that were used to generate data for fitting $H(\theta)$.

The resulting retina thickness curves, as a function of micrometers from the center of the fovia, are shown below in Figure 3a. After the data was gathered, MATLAB's *CurveFit* toolbox was used to find the optimal parameters that fit the following function

$$H(\theta) = a + b\theta e^{-c\theta}$$

to the biological data. This form of $H(\theta)$ was chosen because the geometry of thickness of the retina increases sharply close to the fovia before decreasing as the distance from the fovia increases. The resulting fit and parameter values are shown in Figure 3b. The final function $H(\theta)$ was used to fit the proposed model to biological data, discussed below in the Results section.

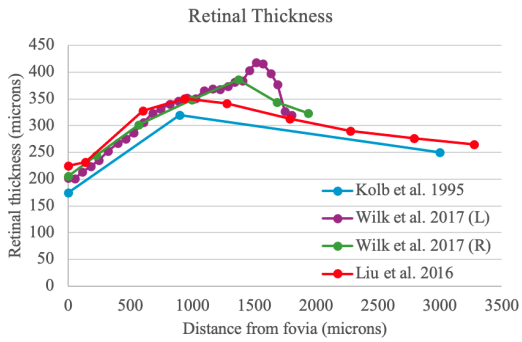

(a) All data used to fit $H(\theta)$.

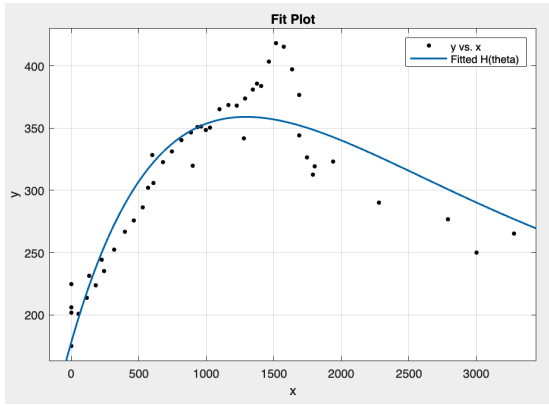

(b) Resultant fit for $H(\theta) = a + b\theta e^{-c\theta}$. The final parameters were $a = 177.7$, $b = 0.0007725$, and $c = 0.3807$.

Figure 3: Fitting $H(\theta)$ to biological data.

2.3 Variants of the $l(\theta)$ Function

Using a modified version of the code from D. M. Anderson, Brager, and Kearsley 2024, we investigated the introduction of a spatial dependence for l_{rH} and l_{cH} by assuming first that $\alpha_1 = \alpha_3$ and $\alpha_2 = \alpha_4$ which aligns with $l_{rH} = l_{cH}$. As a base case, we assume that $\alpha_2 = 0$ to align with the biological necessity of a non-negative retinal thickness. For this to occur, it is required that $0 \leq \alpha_2 \leq \frac{1}{\max\limits_{\theta>0} H(\theta)}$. Since $H(\theta)$ is on the order of the hundreds in terms of our measurements of microns, $\alpha_2 = 0$ is a reasonable assumption. Thus, the dependence of maximum OS length and retinal thickness is linear. To compare with the results of the original adaptation of the model, we optimize four different parameters: $p_r = \frac{\mu_r}{a_r}$, $p_c = \frac{\mu_c}{a_c}$, β, and α_1. Following D. M. Anderson, Brager, and Kearsley 2024, we set $\gamma = 0$ since incorporating theta into maximum length is not expected to affect the dependence of nutrient concentration on cone population. Figure 4 displays the optimized results for an initial guess of $[p_r, p_c, \beta, \alpha_1]$= [77.5, 77.5, 0.0036, 82.9]. The values for the predicted parameters are [1.022, 1.022, 1.2445, 0.4857]. It is notable that $\alpha_1 = 0.4857$ since it is biologically realistic to say that the maximum OS length is less than the retinal thickness, so this fractional value is reasonably restricting. Figure 5 demonstrates the results for the same initial guess assuming that the values for l_{rH} and l_{cH} are independent of theta, as assumed in the prior version of this model. In the optimization scheme, a constant parameter value $l*$ such that $\bar{l}_{rH} = \bar{l}_{cH} = \bar{l}$ is optimized as opposed to α_1. Notably, the parameter optimization is not unique for these four parameters, but it is along a unique manifold. For the specific graphs, shown here, the parameters are approximately $[p_r, p_c, \beta, \bar{l}]$= [89.0, 89.0, 0.0002, 89.9], but the manifold values as reported in Table 6 of D. M. Anderson, Brager, and Kearsley 2024 are $\bar{l} - p = 0.83$, $\beta p^2 = 1.5$, and $\frac{\gamma}{\beta} = 0$. While it is evident that the first of these values does not apply to the linear model, it is possible that the other two have some connection. For the linear model, $\beta p^2 = 1.5$ and $\frac{\gamma}{\beta} = 0$. The latter is consistent with the constant model trivially, but the closeness of the βp^2 value is worth considering during future investigation.

The model with linear spatial dependence of retinal thickness on maximum photoreceptor OS length results in a worse fit to the biological data (Figure 4, upper right) than assuming constant dependence (Figure 5, upper right). However, there are qualities of the linear spatial dependent model that are desirable. For example, in the model with $l_{rH} = l_{cH} = \alpha_1$, photoreceptor OS length increases as it approaches points far away from the fovia after it reaches a minimum value at approximately $\theta = 0.4$. The retinal thickness is known to be low (30-80 microns) at larger values of θ. It is unlikely that the rod OS length would be 30 microns in this area as the constant prediction suggests. While the the model with linear dependence $l_{rH} = l_{cH} = \alpha_1 H(\theta)$ shows this same type of behavior, the OS length at large θ is less than 20 microns, which is likely more biologically accurate. Additionally, the data gathered during the process of fitting $H(\theta)$ as well as from D. M. Anderson, Brager, and Kearsley 2024 suggests that an inverse relationship between OS length and retinal thickness is possible for small theta values, while

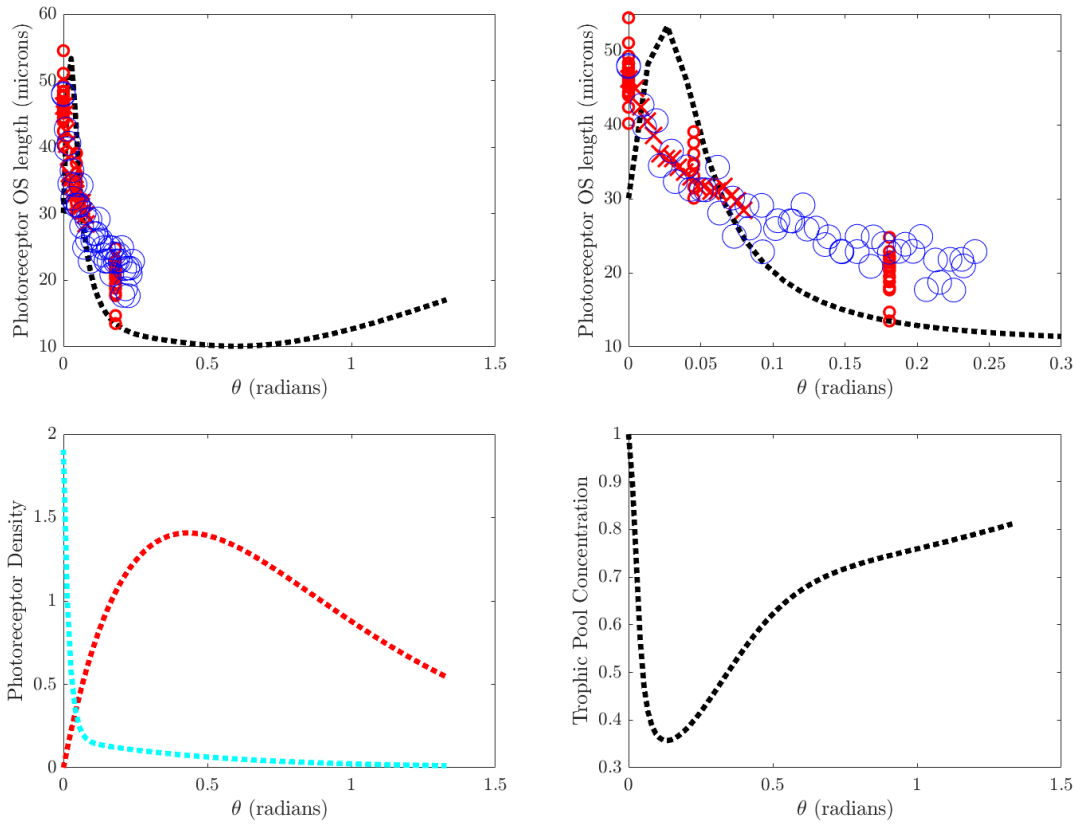

Figure 4: Linear spatial dependence as a function of retina thickness. In subfigure 1, the small red circles at $\theta = 0$ are the 'maximum' OS lengths reported in Wilk et al. 2017 Table 1. The small red circles at $\theta = \theta_{0.5mm}$ are the 'minimum' OS lengths reported in Wilk et al. 2017 Table 1. The small red circles at $\theta = \theta_{2.0mm}$ are the 2 mm OS lengths reported in Wilk et al. 2017 table 1. The crosses are the points used from Wilk et al. 2017 in the objective function to minimize the least square error. The large blue circles are collectively the points from Wilk et al. 2017 subject with low peak density and subject with the highest peak density shown for reference but otherwise not used in the optimization problem. The black dotted line represents in each plot the numerical solution when the diffusion coefficient is 0. Subfigure 2 is a zoomed-in-version of Subfigure 1. Subfigure 3 shows the rod and cone densities as a function of θ (distance in radians from the fovea) for a human retina based on data from Curcio et al. 1990 and Roberts et al. 2017. The red lines show the rod densities and the cyan lines show the cone densities. Subfigure 4 represent the RPE concentration. The optimized parameter values used in this are: p_r=1.0220, p_c=1.0220, β=1.2445, γ=0, α_1=0.4857.

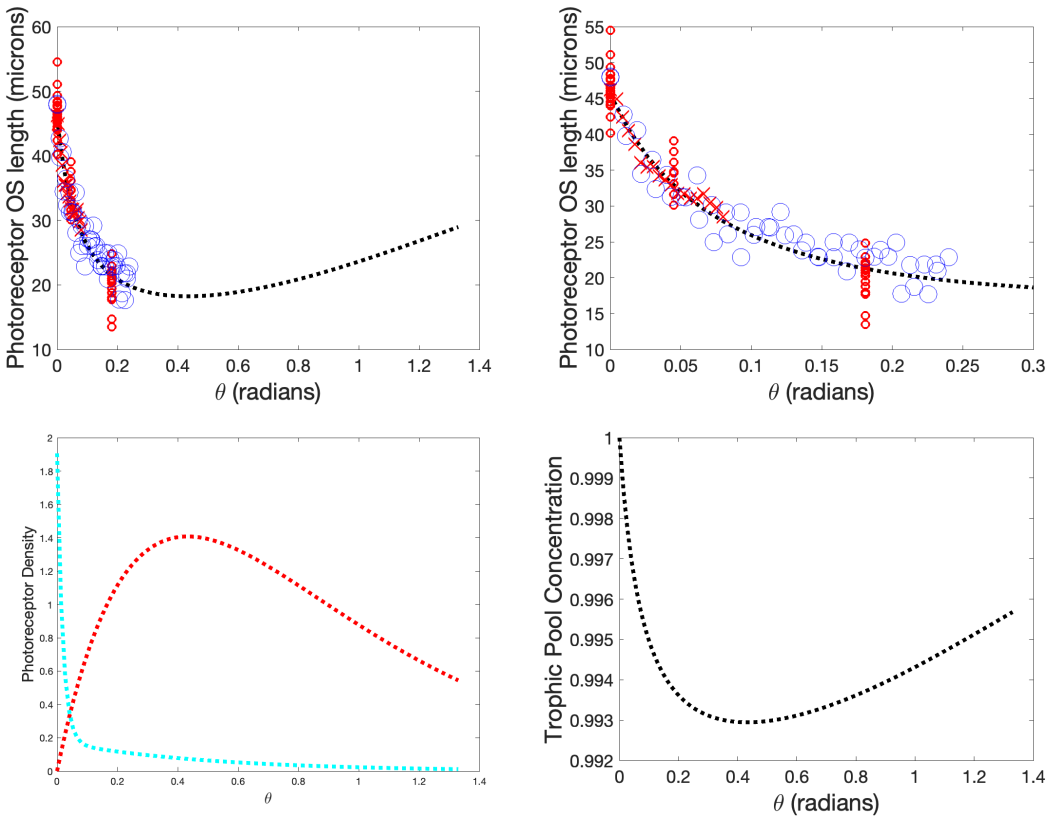

Figure 5: For constant $l_{rH} = l_{cH}$. In subfigure 1, the small red circles at $\theta = 0$ are the 'maximum' OS lengths reported in Wilk et al. 2017 Table 1. The small red circles at $\theta = \theta_{0.5mm}$ are the 'minimum' OS lengths reported in Wilk et al. 2017 Table 1. The small red circles at $\theta = \theta_{2.0mm}$ are the 2 mm OS lengths reported in Wilk et al. 2017 table 1. The crosses are the points used from Wilk et al. 2017 in the objective function to minimize the least square error. The large blue circles are collectively the points from two Wilk et al. 2017 subjects, one with low peak density and and one with the highest peak density, both shown for reference but otherwise not used in the optimization problem. The black dotted line represents the numerical solution with optimized parameters. Subfigure 2 is a zoomed-in-version of Subfigure 1. Even though only the crosses are used in the objective function, the approximation matches the other data points well. Subfigure 3 shows the rod and cone densities as a function of θ (distance in radians from the fovea) for a human retina based on data from Curcio et al. 1990 and Roberts et al. 2017. The red lines show the rod densities and the cyan lines show the cone densities. Subfigure 4 represents the RPE concentration. The optimized parameter values used in this are: p_r=89.0297, p_c=89.0343, β=0.0002, γ=0, $\bar{l}$=89.8574.

later theta values demonstrate a more linear relationship. Thus, the poor performance for small theta is expected, and the linear relationship may be more accurate if just larger values of theta are considered. A logistic function of $H(\theta)$ is suspected to capture the important behavior of this relationship.

Though we were unable to fit the model for the case where l_{rH} and l_{cH} are logistically constrained by $H(\theta)$, we discuss this as a direction for figure work below in Section 4.

2.4 Analysis for Model 1

2.4.1 Nondimensionalized Model

We define the following non-dimensionalized relations:

$$\bar{r} = \frac{r}{l_{rH}} \quad \bar{c} = \frac{c}{l_{rH}} \quad \bar{T} = \frac{Tk}{\Gamma} \quad \bar{R} = R(l_{rH})^2 \quad \bar{C} = C(l_{cH})^2 \quad \bar{\mu_r} = \frac{\mu_r}{\Gamma}$$
$$\bar{\mu_c} = \frac{\mu_c}{\Gamma} \quad \bar{t} = t\Gamma \quad \bar{\beta} = \frac{\beta}{\Gamma} \quad \bar{\gamma} = \frac{\gamma}{\Gamma} \quad \bar{a_r} = \frac{a_r l_{rH}}{k} \quad \bar{a_c} = \frac{a_c l_{cH}}{k}$$

Hence our nondimensionalized model becomes:

$$\frac{\partial \bar{r}}{\partial \bar{t}} = \bar{a_r}\bar{r}\left(1-\bar{r}\right)\bar{T} - \bar{\mu_r}\bar{r} \tag{4}$$
$$\frac{\partial \bar{c}}{\partial \bar{t}} = \bar{a_c}\bar{c}\left(1-\bar{c}\right)\bar{T} - \bar{\mu_c}\bar{c} \tag{5}$$
$$\frac{\partial \bar{T}}{\partial \bar{t}} = \bar{T}\left[(1-\bar{T}) - \bar{\beta}\bar{R}(1-\bar{r})\bar{r} - \bar{\gamma}\bar{C}(1-\bar{c})\bar{c}\right] \tag{6}$$

2.4.2 Steady state Solution

There is the trivial steady state $(0,0,0)$ and to denote one of the non-trivial steady states (r^*, c^*, T^*), we have obtained it as follows:

Considering the non-dimensionalized form for $\bar{r}$, for steady states, let the right-hand side of Equation (4) equals to zero. We can obtain that $\bar{r}^* = 0$ or $\bar{r}^*$ satisfying the following equation:

$$\bar{a_r}\left(1-\bar{r}\right)\bar{T} - \bar{\mu_r} = 0$$

Solving for the equation above, we find that $\bar{r}^* = 1 - \dfrac{\bar{\mu_r}}{\bar{a_r}\bar{T}}$.

Similarly, for $\bar{c}$, we can get $\bar{c}^* = 0$ or we must find $\bar{c}^*$ through the following equation:

$$\bar{a_c}\left(1-\bar{c}\right)\bar{T} - \bar{\mu_c} = 0$$

Solving for the equation above, we find that $\bar{c}^* = 1 - \dfrac{\bar{\mu_c}}{\bar{a_c}\bar{T}}$.

Considering the non-dimensionalized form for $\bar{T}$, $\bar{T}^* = 0$ or we must find $\bar{T}^*$ through the following equation:

$$(1-\bar{T})-\bar{\beta}\bar{R}(1-\bar{r})\bar{r}-\bar{\gamma}\bar{C}(1-\bar{c})\bar{c}=0$$

Giving a perturbation to T, we set $\bar{T}\approx 1+\epsilon$ with the assumption $\epsilon << 1$. We arrive at the following dimensionless form for ϵ after a **bit** of algebra:

$$\epsilon=\frac{-\bar{\beta}\bar{R}(\theta)\bar{\mu_r}\bar{a_c}^2\bar{a_r}+\bar{\beta}\bar{R}(\theta)\bar{\mu_r}^2\bar{a_c}^2-\bar{\gamma}\bar{C}(\theta)\bar{\mu_c}\bar{a_r}^2\bar{a_c}+\bar{\gamma}\bar{C}(\theta)\bar{\mu_c}^2\bar{a_r}^2}{\bar{a_r}^2\bar{a_c}^2+\bar{\beta}\bar{R}(\theta)\bar{\mu_r}\bar{a_c}^2\bar{a_r}+\bar{\gamma}\bar{C}(\theta)\bar{\mu_c}\bar{a_r}^2\bar{a_c}} \tag{7}$$

After dimensionalizing by spatial dependence, we get:

$$\epsilon(\theta)=\frac{-\bar{\beta}R(\theta)\bar{\mu_r}{a_c}^2a_rl_{rH}(\theta)k+\bar{\beta}R(\theta)\bar{\mu_r}^2{a_c}^2k^2-\bar{\gamma}C(\theta)\bar{\mu_c}{a_r}^2a_cl_{cH}(\theta)k+\bar{\gamma}C(\theta)\bar{\mu_c}^2{a_r}^2k^2}{{a_r}^2{a_c}^2+\bar{\beta}R(\theta)\bar{\mu_r}{a_c}^2a_rl_{rH}(\theta)k+\bar{\gamma}C(\theta)\bar{\mu_c}a_r{}^2a_cl_{cH}(\theta)k} \tag{8}$$

Setting the parameter set equal to the parameters listed in (D. M. Anderson, Brager, and Kearsley 2024), we find that $r, c, T,$ and ϵ is equal to:

$$r^*=r_0\left[l_{rH}(\theta)-\frac{p_r}{1+\epsilon(\theta)}\right] \tag{9}$$

$$c^*=c_0\left[l_{cH}(\theta)-\frac{p_c}{1+\epsilon(\theta)}\right] \tag{10}$$

$$T^*\approx\frac{\Gamma}{k}\left[1+\epsilon(\theta)\right] \tag{11}$$

$$\epsilon(\theta)=\frac{\beta p_r\bar{R}(\theta)\left[-\bar{l}_{rH}(\theta)+p_r\right]+\gamma p_c\bar{C}(\theta)\left[-\bar{l}_{cH}(\theta)+p_c\right]}{1+\beta p_r\bar{R}(\theta)\bar{l}_{rH}+\gamma p_c\bar{C}(\theta)\bar{l}_{rH}} \tag{12}$$

where

$$\bar{R}(\theta)=\frac{R(\theta)}{R_{max}},\quad \bar{C}(\theta)=\frac{C(\theta)}{C_{max}},\quad \bar{l}_{rh}=\frac{l_{rh}}{r_0},\quad \bar{l}_{ch}=\frac{l_{ch}}{c_0},\quad p_r=\frac{\mu_r}{a_r},\quad p_c=\frac{\mu_c}{a_c} \tag{13}$$

while R_{max} and C_{max} are the maximum rod and cone densities. r_0 and c_0 represent the healthy reference values for outer segment lengths of rods and cones (D. M. Anderson, Brager, and Kearsley 2024).

3 Model 2

3.1 Proposed Model

The following inquiry is inspired by the data presented in Figure 6 that came from Christopher J. Guerin and D. H. Anderson 1993. The data was obtained by detaching the retina inside the eye (which causes rods and cones to die), then allowing it to reattach and monitoring the regrowth process for the cones and rods.

We observe that the distribution of the photoreceptive cells over length is evolving in time, by first propagating towards higher values of l, and then settling in what appears to be an equilibrium distribution. We will postulate a simple PDE model for this process, simulate it by discretizing the PDE and compare our results with the experimental data.

To model the evolution of the cell density function we propose a simple advection-diffusion model over the length space:

$$\frac{\partial \rho}{\partial t} + \frac{\partial}{\partial l}\left(a(l)\rho - D\frac{\partial \rho}{\partial l}\right) = 0 \quad l \in \left(0, \hat{L}\right) \tag{14a}$$

$$a(l)\rho(l,t) - D\frac{\partial \rho(l,t)}{\partial l}\Big|_{l=0,\hat{L}} = 0 \tag{14b}$$

$$\rho(l,0) = \rho_0(l) \tag{14c}$$

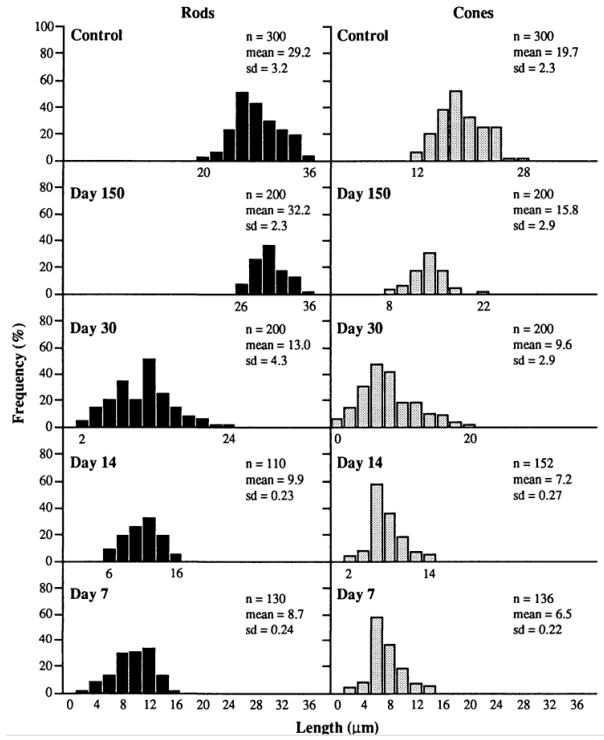

Figure 6: Experimental Data

The advection term in the PDE above simulates the growth of the cells over time, which is the main effect we are interested in; meanwhile, the diffusion term models random fluctuations in the growth of the cones and rods.

The boundary condition (14b) is chosen to conserve the total number of cones/rods: by integrating both sides of the PDE (14a) we get

$$\frac{\partial}{\partial t}\int_0^{\hat{L}} \rho \, dl + \left[a(l)\rho - D\frac{\partial \rho}{\partial l}\right]_0^{\hat{L}}, = 0$$

so with the boundary condition (14b) we indeed have conservation of the number of cells.

Finally, as we expect the cell growth to be roughly logistic, we choose the flux function $a(l)$ to be

$$a(l) = l(1 - l/l_{\max}), \tag{15}$$

where $l_{\max}$ is the optimal length of the cones/rods.

The initial boundary value problem (14) was discretized using the standard finite element method in space and the implicit-explicit Crank-Nicolson leapfrog method in time.

3.2 Numerical Solution

The results of a numerical simulation of the model are presented in Figure 7 below. We see that the result of our model has the same qualitative behaviour as the experimental data, namely it predicts that the cells grow to a certain length, and then stabilize in a normal-like distribution around it.

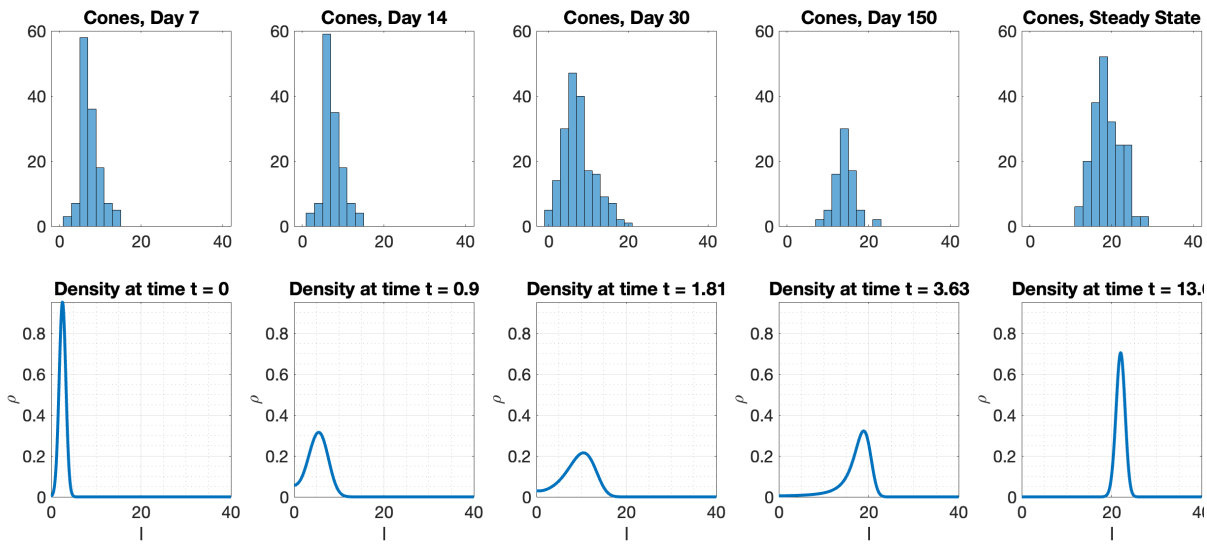

Figure 7: Top row: experimental data.
Bottom row: results of a numerical simulation

4 Conclusions

In this study, we developed two models about the outer segment length of photoreceptors. Model 1 is based on the PDE model from D. M. Anderson, Brager, and Kearsley 2024 including the influence of the retinal thickness on the length scale of photoreceptors' outer segment length. By analyzing the data from Kolb, Fernandez, and Nelson 1995; Wilk et al. 2017; Liu, Kocaoglu, and Miller 2016, we obtained a function of retinal thickness with spatial dependence. We first assumed that the outer segment length scales are linear related to the retinal thickness. By simulating the spatial dependence of outer segment length, we were able to determine optimal parameters for the model and compare those with the constant case.

We also developed a method to validate the new PDE-based model about the outer segment length of photoreceptors with perturbation analysis for steady states. Firstly, we normalized the model with dimensionless variables. In particular, we can find the expression of steady states. By finding the equilibrium in the normalized version of PDE system, we can use a perturbation to test the system. With this perturbation analysis, we can verify the model with the values of parameters and the setting of the spatial dependence of densities of photoreceptors.

For the second model, we built an advection-diffusion model to describe the density function of photoreceptors with different lengths at different times. This PDE system is based on the combination of the shedding and growing mechanics of the photoreceptors and the Fokker-Planck equation. By this model, we reproduced the experimental results from Christopher J. Guerin and D. H. Anderson 1993.

4.1 Directions for Future Work

When fitting Model 1 to biological data, we tested simple cases where OS length was independent of $H(\theta)$ and linear related to $H(\theta)$. However, evidence from images of the retina from previous research suggests that retina thickness and OS length are inversely related. So, in the future, we would like to fit the original Model 1, where l_{rH} and l_{cH} depend logistically on $H(\theta)$, to biological data as well. The logistical dependence ensures that l_{rH} and l_{cH} are constrained by the retinal thickness (as is the case in the retina) but allows for the OS segment lengths (r and c) to be inversely related to the retinal thickness.

Additionally, for Model 1, we have two steady states for future work to focus on. The first point to focus on is to fit the steady-state solutions into the data-fitting model. From there, we should expect a trivial solution with $r^* = c^* = T^* = 0$ and a nontrivial solution with the nontrivial values we solved for in the Model 1 Analysis Section. With our nontrivial solution, we require the parameters to be optimized to fit Model 1. Currently, we are using a linear relationship between the retinal thickness and the maximum OS length attainable in the absence of other influences, so letting $\alpha_2 \neq \alpha_4 \neq 0$ in the optimization is the next variant to explore. The second point to focus on is performing stability analysis on the new model. This involves finding the Jacobian of the system and evaluating the Jacobian at each steady state to determine the behaviour of the system at each state. This information is relevant as it gives insight into how the proposed model reacts to small perturbations around these states. An unstable steady state might result in the system (model) becoming chaotic. If the system is unstable, the original relationship between photoreceptor OS length and θ no longer holds within this particular model. Lastly, we can note that an unstable system might need to go through either further analysis or a suggested new model.

Stability analysis is also important information to note due to the data fitting model used in D. M. Anderson, Brager, and Kearsley 2024, which describes that photoreceptor OS length will decrease, then increase as θ (radians) increases from 0.

The work on Model 2 can be continued by allowing for the cells to be added to the system by modifying the boundary condition at $l = 0$, improving the numerical scheme to make it more stable, and adding a shedding term to make the model more realistic.

References

Roberts, Paul A. et al. (2017). "Mathematical models of retinitis pigmentosa: The oxygen toxicity hypothesis". In: *Journal of Theoretical Biology* 425, pp. 53–71. ISSN: 0022-5193. DOI: https://doi.org/10.1016/j.jtbi.2017.05.006. URL: https://www.sciencedirect.com/science/article/pii/S002251931730214X.

photoreception (n.d.). https://www.britannica.com/science/photoreception. Accessed: 2024-06-22.

Roberts, Paul A. (2022a). "Mathematical models of retinitis pigmentosa: The trophic factor hypothesis". In: *Journal of Theoretical Biology* 534, p. 110938. ISSN: 0022-5193. DOI: https://doi.org/10.1016/j.jtbi.2021.110938. URL: https://www.sciencedirect.com/science/article/pii/S002251932100357X.

— (2022b). "Inverse Problem Reveals Conditions for Characteristic Retinal Degeneration Patterns in Retinitis Pigmentosa Under the Trophic Factor Hypothesis". In: *Frontiers in Aging Neuroscience* 14. ISSN: 1663-4365. DOI: 10.3389/fnagi.2022.765966. URL: https://www.frontiersin.org/articles/10.3389/fnagi.2022.765966.

Camacho, Erika T and Stephen Wirkus (2013). "Tracing the progression of retinitis pigmentosa via photoreceptor interactions". In: *Journal of theoretical biology* 317, pp. 105–118.

Anderson, Daniel M., Danielle C. Brager, and Anthony J. Kearsley (2024). "Spatially-dependent model for rods and cones in the retina". In: *Journal of Theoretical Biology* 579, p. 111687. ISSN: 0022-5193. DOI: https://doi.org/10.1016/j.jtbi.2023.111687. URL: https://www.sciencedirect.com/science/article/pii/S0022519323002849.

Wilk, Melissa A et al. (2017). "Evaluating outer segment length as a surrogate measure of peak foveal cone density". In: *Vision Research* 130, pp. 57–66.

Kolb, Helga, Eduardo Fernandez, and Ralph Nelson (1995). "Webvision: the organization of the retina and visual system [Internet]". In.

Liu, Zhuolin, Omer P Kocaoglu, and Donald T Miller (2016). "3D imaging of retinal pigment epithelial cells in the living human retina". In: *Investigative ophthalmology & visual science* 57.9, OCT533–OCT543.

Curcio, Christine A et al. (1990). "Human photoreceptor topography". In: *Journal of comparative neurology* 292.4, pp. 497–523.

Christopher J. Guerin Geoffrey P. Lewis, Steven K. Fisher and Don H. Anderson (1993). "Recovery of Photoreceptor Outer Segment Length and Analysis of Membrane Assembly Rates in Regenerating Primate Photoreceptor Outer Segments". In: *Iiivestigative Ophthalmology & Visual Science* 34, pp. 175–183. ISSN: 1552-5783. DOI: https://iovs.arvojournals.org/article.aspx?articleid=2179081. eprint: https://arvojournals.org/arvo/content_public/journal/iovs/933395/175.pdf.